


Measuring Concurrence in Qubit Werner States Without an Aligned Reference Frame

Kateřina Jiráková^{1,*}, Artur Barasiński^{1,2,†}, Antonín Černocho^{1,‡}, Karel Lemr^{1,§} and Jan Soubusta^{3,¶}

¹*Joint Laboratory of Optics of Palacký University and Institute of Physics of Czech Academy of Sciences, 17. listopadu 12, Olomouc 771 46, Czech Republic*

²*Institute of Theoretical Physics, University of Wrocław, Plac Maxa Borna 9, 50-204 Wrocław, Poland*

³*Institute of Physics of the Czech Academy of Sciences, Joint Laboratory of Optics of PU and IP AS CR, 17. listopadu 50A, Olomouc 772 07, Czech Republic*

 (Received 13 May 2021; revised 25 June 2021; accepted 14 October 2021; published 23 November 2021)

The genuine concurrence is a standard quantifier of multipartite entanglement, detection, and quantification of which still remains a difficult problem from both the theoretical and experimental points of view. Although many efforts have been devoted to the detection of multipartite entanglement (e.g., using entanglement witnesses), measuring the degree of multipartite entanglement, in general, requires some knowledge about the exact shape of a density matrix of the quantum state. An experimental reconstruction of such a density matrix can be done by full state tomography, which amounts to having the distant parties share a common reference frame and well-calibrated devices. Although this assumption is typically made implicitly in theoretical works, establishing a common reference frame, as well as aligning and calibrating measurement devices in experimental situations, are never trivial tasks. It is therefore an interesting and important question whether the requirements of having a shared reference frame and calibrated devices can be relaxed. In this work, we study both theoretically and experimentally the genuine concurrence for the generalized Greenberger-Horne-Zeilinger states under randomly chosen measurements on individual qubits without a shared frame of reference and calibrated devices. We present the relation between genuine concurrence and the so-called nonlocal volume, a recently introduced indicator of nonlocality.

DOI: [10.1103/PhysRevApplied.16.054042](https://doi.org/10.1103/PhysRevApplied.16.054042)

I. INTRODUCTION

Secure and reliable information exchange is of paramount importance worldwide, hence the practical implementation of quantum communications protocols outside the scientific laboratory has become one of the main focuses of recent studies [1,2]. Naturally, such advances in quantum communication methods require the ability to perform quantum measurements in an unstable environment, where the strict requirements for alignment and calibration of remote devices are hard to meet (e.g., long-distance quantum communication [3–5] or satellite-based communications [6–9]). Specifically, the above-mentioned quantum communications experiments usually rely on quantum optical devices, where qubits are encoded into polarization states of light. However, this necessarily

requires a common reference measurement frame to be shared that has to be well aligned and calibrated measurement devices (in a sense of well-defined scale of measurement apparatus such as the rotation angles of wave plates). Furthermore, it also needs to be maintained stable for the entire experiment or communication. From an experimental point of view, this is, however, never achieved without technical difficulties (see, for instance, [10]). Maintaining a common reference frame seems a trivial assumption when confined to a laboratory, but long-distance quantum communications beyond the Earth's surface [6–9] have already led scientists to re-evaluate the practicality of such an assumption [11,12].

A possible solution to these problems in free space could be to use rotationally invariant states of light [13]. However, no one has yet applied these solutions in satellite quantum communication. Instead, much attention has been paid to so-called reference-frame-independent (RFI) protocols [14–21]. For instance, it was proved in Ref. [22] that a RFI quantum key distribution protocol [23] is more robust under reference frame fluctuations than its standard counterpart [24,25].

*katerina.jirakova@upol.cz

†artur.barasinski@uwr.edu.pl

‡antonin.cernoch@upol.cz

§k.lemr@upol.cz

¶soubusta@fzu.cz

Motivated by all these observations, in this paper we also investigate the RFI approach. In particular, we focus on quantum entanglement, which is undoubtedly the essence of many quantum information procedures [26–28]. Therefore, it is necessary to be able to test for the presence of entanglement and, for the reason explained previously, it is practical to manage it in RFI mode [29–33]. Over time, several methods for entanglement detection under these constraints have been proposed. They are based on various approaches, for example, on the violation of a Bell inequality [34,35], the second moment of the distribution of correlations [36,37], a geometrical threshold criterion [38], or interference between multiple copies of the investigated state [39]. However, all of them were so far limited to being mere witnesses to entanglement rather than measures. Entanglement quantification is of considerable interest for both theoretical and practical reasons. Our goal is to introduce a device-independent entanglement quantification protocol operating in the RFI approach without calibrating measurement devices, which is of great importance from the experimental point of view. More specifically, we investigate the RFI measure of Bell nonlocality and its relation with entanglement. As Bell nonlocality and entanglement are distinct resources, one cannot establish a direct link between them in the general case, and this is the price paid for the great simplification of the experimental requirements given previously. However, such a relationship can be identified for specific families of states. Because of this, we restrict our attention to two- and three-qubit states which are of practical importance in quantum information processes. One such example is the family of Werner states which have been instrumental for various important advancements in quantum information [40–42]. Moreover, the Werner states are “considered as the paradigmatic example of realistic noisy preparation of a pure entangled state subject to the action of white noise” [43]. Although this family contains examples of states with nonclassical correlations, which nevertheless admit a hidden-variable model, the violation of a local-realistic description is still observed for highly entangled cases which are, in fact, applied in quantum information procedures. We also discuss to what extent the results obtained for the Werner states can be used to estimate the entanglement of other two- and three-qubit states. In other words, we test how precisely one can estimate the entanglement of an unknown state if our RFI approach is applied. Surprisingly, we found that our calculations can be successfully applied to quantify the entanglement of more general states, for example, pure states, Greenberger-Horne-Zeilinger (GHZ) symmetric states. This result also justifies the experimental simplification within which we still obtain an instrument that can find its application in future practical long-distance quantum communications. Finally, we present an experimental verification of our predictions.

II. PRELIMINARIES

A. Entanglement measure

We now introduce concepts that are relevant to the current investigation. Let us first consider a two-qubit pure state $|\psi\rangle_2$, composed of subsystems A and B . The degree of entanglement between both subsystems is given by so-called *concurrence* [44], $\mathcal{C}(|\psi\rangle_2) = \sqrt{2(1 - \text{Tr}(\rho_A^2))}$, where ρ_A denotes the reduced density matrix of subsystem A . For mixed states ρ the concurrence is defined by the convex-roof extension [45], $\mathcal{C}(\rho) = \min_{\text{all decomp.}} \sum_j p_j \mathcal{C}(|\psi_j\rangle)$, where the minimum average concurrence is taken over all possible convex decompositions $\rho = \sum_j p_j |\psi_j\rangle\langle\psi_j|$ into pure states. In a special case, when ρ_2 denotes a two-qubit mixed state, the mixed-state concurrence is given by

$$\mathcal{C}(\rho_2) = \max\{0, \sqrt{\lambda_1} - \sum_{j=2}^4 \sqrt{\lambda_j}\} \quad (1)$$

with $\{\lambda_j\}$ being the decreasingly ordered eigenvalues of $\rho_2(\sigma^y \otimes \sigma^y)\rho_2^T(\sigma^y \otimes \sigma^y)$, where σ^y denotes the Pauli matrix and the transposition is performed in any product basis.

The measure described previously can be further extended to describe the genuine multipartite entanglement (GME) [46–49], that is, a scenario when a multipartite state has a minimum amount of entanglement in each bipartition. For instance, if the analyzed pure state $|\psi\rangle_3$ is composed of three subsystems A , B , and C , one can distinguish three bipartitions $\{\gamma|\gamma'\}$, namely $\{A|BC\}$, $\{B|AC\}$, and $\{C|AB\}$. Then, the GME concurrence is given by [48]

$$\mathcal{C}_{\text{GME}}(|\psi\rangle_3) = \min_{\text{all bipart.}} \sqrt{2(1 - \text{Tr}(\rho_\gamma^2))}, \quad (2)$$

where the minimum is taken over all possible bipartitions $\{\gamma|\gamma'\}$ and ρ_γ denotes the corresponding reduced density matrix of subsystem γ . The extension of GME concurrence to mixed states also follows the convex-roof extension presented previously [48].

We stress that a general expression for mixed-state GME concurrence still remains unknown. However, it has been successfully evaluated for the so-called X-matrix states [50]. These states are represented by a density matrix written in an orthonormal product basis, the nonzero elements of which are only the diagonal (denoted by a_j and b_j , where $j = \{1, \dots, 2^{N-1}\}$) and/or antidiagonal elements (given by z_j and its conjugation). The X-matrix states are positive if $|z_j| \leq \sqrt{a_j b_j}$ and we also expect $\sum_j (a_j + b_j) = 1$ to ensure the normalization of ρ_X . The GME concurrence for these states is given by [51]

$$\mathcal{C}_{\text{GME}}(\rho_X) = 2 \max_i \{0, |z_i| - \chi_i\}, \quad (3)$$

where $\chi_i = \sum_{j \neq i} \sqrt{a_j b_j}$.

B. Bell-nonlocal correlations

Next, let us consider an N -partite Bell experiment where each party has a choice over two measurement settings $S_i = \{0, 1\}$ and each measurement results in one of two possible outcomes $r_i = \{0, 1\}$. The corresponding Bell experiment is then fully characterized by the set of joint conditional probability distributions $\mathbf{P} = \{P(\vec{r}_N | \vec{S}_N)\}$, where $\vec{r}_N = (r_1, \dots, r_N)$ and $\vec{S}_N = (S_1, \dots, S_N)$. When the participants share a quantum state ρ and the correlations are generated by local measurements performed on their respective subsystems, then \mathbf{P} takes the form of $P(\vec{r}_N | \vec{S}_N) = \text{Tr} \left(\bigotimes_{i=1}^N \hat{M}_{r_i | S_i} \rho \right)$, where $\hat{M}_{r_i | S_i}$ is the positive operator-valued measure representing the measurement on the i th party with measurement settings S_i .

To make it evident whether a given \mathbf{P} can be described by a local realistic description, one can employ a linear function of probabilities called the Bell inequality [52]. It can be written as

$$\mathcal{I}(\mathbf{P}) \equiv \sum_{\vec{r}_N, \vec{S}_N} \mu_{\vec{r}_N}^{\vec{S}_N} P(\vec{r}_N | \vec{S}_N) \leq C_{\text{LHV}}, \quad (4)$$

where $\{\mu_{\vec{r}_N}^{\vec{S}_N}\}$ are real coefficients and C_{LHV} refers to the upper threshold of $\mathcal{I}(\mathbf{P})$ for the local realistic description. Consequently, if one observes a value of $\mathcal{I}(\mathbf{P})$ greater than C_{LHV} , the correlations are said to be Bell nonlocal. The value of coefficients $\{\mu_{\vec{r}_N}^{\vec{S}_N}\}$ solely depends on the analyzed model of local realistic description [53–56]. For instance, when $N = 2$ the Bell experiment [Eq. (4)] is characterized by the Clauser-Horne-Shimony-Holt (CHSH) inequality [53]. On the other hand, when $N = 3$ the genuine multipartite nonlocal correlations discussed in this paper require the consideration of a set of 185 Bell inequalities defined in Ref. [56].

The presence of Bell-nonlocal correlations clearly certifies the presence of entanglement, and this conclusion follows regardless of how \mathbf{P} is generated from the underlying state and measurements. Therefore, Eq. (4) is said to be a device-independent witness for entanglement [57]. The relation between entanglement and Bell nonlocality has been studied intensively. For instance, in Ref. [58] the authors showed that $\mathcal{C}(|\psi\rangle_2) = \sqrt{\beta_2^2 - 1}$, where β_2 denotes the maximal violation of the CHSH inequality [53]. Similar investigations have been performed for three-qubit states (see, for instance, [59,60] and [61] for an experimental demonstration).

Nevertheless, the previously described demonstration of nonlocal correlations employs carefully chosen measurements the implementation of which requires the spatially separated observers to share a complete reference frame

and well-calibrated devices. Although this assumption is typically made implicit in theoretical works, establishing a common reference frame, as well as aligning and calibrating measurement devices in experimental situations are never trivial tasks. Recently, Liang *et al.* [34] have proposed a reference-frame-independent protocol to circumvent the previously mentioned problem. In their approach, the following quantity is considered [34,62]

$$p_V(\rho) = \int \omega(\rho, \Omega) d\Omega, \quad (5)$$

where the integration comprises a space of measurement parameters Ω according to the Haar measure. The function $\omega(\rho, \Omega)$ is an indicator function that takes the value 1 whenever the generated behavior is nonlocal and 0 otherwise. Importantly, in this approach the nonlocal correlations are quantified without any prior assumptions about specific Bell inequalities [35,63,64]. In other words, the generated behavior is nonlocal if at least one inequality of the suitable set of Bell inequalities is violated. The quantity p_V , if properly normalized, can be interpreted as a probability of violation of local realism for the measurement operators $\hat{M}_{r_i | S_i}$ sampled randomly according to the Haar measure. To avoid confusion, we prefer to use the unique term nonlocal fraction [63] to describe the quantity p_V .

III. DEVICE-INDEPENDENT ESTIMATION OF ENTANGLEMENT

In this paper we consider a source producing copies of an unknown N -qubit state ρ_{in} , which is transmitted through randomly unitary evolving quantum channels to N local observers. During the j th transmission the state ρ_{in} is transformed by N random local unitary operators $U_i^{(j)}$ according to

$$\rho_{\text{out}} = \bigotimes_{i=1}^N U_i^{(j)} \rho_{\text{in}} \bigotimes_{i=1}^N U_i^{(j)\dagger}. \quad (6)$$

We assume that the unitary transformation has a timescale that is sufficiently slow to obtain stable measurements for given projections together with their orthogonal counterparts, but the transformation is much faster to apply standard techniques of state analysis [65]. In other words, we can reliably accumulate signal for one particular measurement setting and its orthogonal-projection counterpart, but not for all the measurement settings in a row. As the local unitary transformations remain unknown, it is clear that a common reference frame cannot be established for the described scenario, nor can local devices be calibrated.

We discuss the entanglement assessment protocol of the input state ρ_{in} based on the nonlocal correlations revealed by the output state ρ_{out} . As the unitary operators during the j th transmission remain unknown for the observers,

the maximal violation of Bell inequalities cannot be determined. Instead, we estimate the nonlocal fraction which is invariant under local unitary transformations applied by each party on the state if one uses the Haar measure for the integration [63]. However, the use of the nonlocal fraction has an important disadvantage which is the lack of analytical solutions [34,63] and, so, the numerical calculations are used to determine the nonlocal fraction.

A. Quantifying bipartite entanglement

1. Two-qubit Werner-like states

First, we consider the scenario when the input state is given in a form of an arbitrary two-qubit pure state $|\theta\rangle_2 = \cos\theta|00\rangle + \sin\theta|11\rangle$ subjected to white noise:

$$\rho_2(\theta, v) = v|\theta\rangle_2\langle\theta| + \frac{1-v}{4}\mathbb{1}_4, \quad (7)$$

where $\mathbb{1}_4$ is the 4×4 identity matrix, v denotes the state visibility ($0 < v \leq 1$), and we assume without loss of generality that $0 < \theta \leq 45^\circ$. The concurrence is given by

$$\mathcal{C}(\rho_2) = \frac{v(2\sin(2\theta) + 1) - 1}{2}. \quad (8)$$

Such states play an important role in quantum information theory as they directly refer to the states generated at the output of the nonlinear process designed in real experiments based on entangled photons [66,67]. In this context, the white noise which enters Eq. (7) is a good approximation of the imperfections occurring in the experimental setup (see, for instance, [68]).

A particular example of the states in Eq. (7) is the two-qubit Werner state [69], $\rho_2^W(v) = \rho_2(\theta = 45^\circ, v)$ [26,40–42]. For the Werner states, concurrence depends only on the visibility, $\mathcal{C}(\rho_2^W) = (3v - 1)/2$. Therefore, the estimation of this parameter is equivalent to the entanglement measurement.

To do that we calculate the nonlocal fraction. Note that the nonlocal correlations of two-qubit states are fully characterized by the CHSH inequality, assuming the freedom in relabeling all measurement settings and/or outcomes and/or parties [70,71]. By straightforward calculations (see Appendix A) one can show that p_V of the Werner state is

$$p_V(v) = \frac{2\left((1-v^2)\arctan\left(\frac{\sqrt{2v^2-1}}{1-v^2}\right) - 3\sqrt{2v^2-1}\right)}{v^2}, \quad (9)$$

which is a monotonic function of v . In other words, a direct measurement of p_V allows the estimation of visibility and, hence, the value of the concurrence $\mathcal{C}(\rho_2^W)$.

Naturally, for general state [Eq. (7)] the nonlocal fraction depends on both the visibility v and angle θ [see

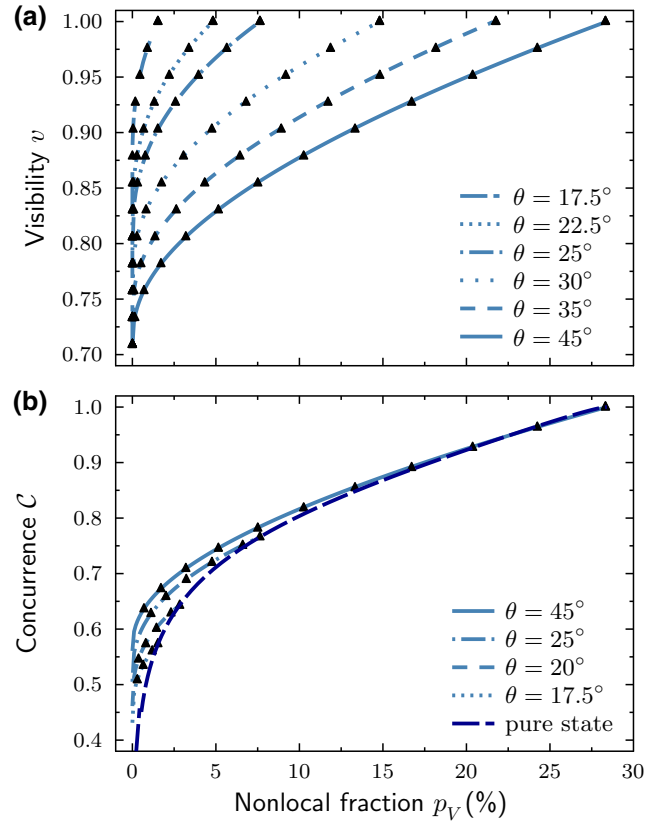


FIG. 1. (a) Visibility and nonlocal fraction for two-qubit Werner-like states given in Eq. (7). Symbols denote numerical results and solid curves correspond to their analytical approximation in Eq. (10). (b) Relation between concurrence \mathcal{C} and nonlocal fraction p_V for two-qubit Werner-like states. As previously, symbols denote numerical results whereas solid curves correspond to analytical approximation.

Fig. 1(a)]. Although the analytical solution of p_V remains unknown in this case, one can always find its approximation. In particular, one can establish the visibility v by

$$v(\theta, p_V) = v_2^{\text{gr}}(\theta) + f_1(\theta)p_V^{1/4} + f_2(\theta)p_V^{1/2} + f_3(\theta)p_V, \quad (10)$$

where

$$\begin{aligned} f_1(\theta) &= (0.19674 - 1.3982\theta + 4.712274\theta^2 \\ &\quad - 6.7193\theta^3 + 3.3384\theta^4)/\sqrt{10}, \\ f_2(\theta) &= 0.11886 - 0.011544\theta^{-1} - 0.363104\theta \\ &\quad + 0.460436\theta^2 - 0.204953\theta^3, \\ f_3(\theta) &= (0.03848 - 0.011\theta^{-1} - 0.02531\theta \\ &\quad - 0.018331\theta^2 + 0.017373\theta^3) \times 10^{-2}, \end{aligned}$$

and $v_2^{\text{cf}}(\theta) = 1/\beta_2$ denotes the critical visibility with the maximal violation of the CHSH inequality $\beta_2 = (\sin^2(2\theta) + 1)^{1/2}$ [58].

As presented in Fig. 1(a), this approximation provides a good agreement with our numerical results. Therefore, substituting Eq. (10) into Eq. (8) one obtains the concurrence $\mathcal{C}(\rho_2)$ depending on the angle θ and the nonlocal fraction p_V [see Fig. 1(b)]. Based on these outcomes, the following remarks can be made.

(i) Whenever an observed $p_V \geq 7\%$, the difference between $\mathcal{C}(\rho_2^W)$ and $\mathcal{C}(\rho_2)$ (hereinafter Δ_2^W) is no greater than 0.02 and vanishes when p_V increases. This means that the concurrence $\mathcal{C}(\rho_2)$ can be estimated (with precision Δ_2^W) assuming that $\rho_2 \equiv \rho_2^W$.

(ii) For $p_V < 7\%$, remark (i) is still valid if $\theta \geq 25^\circ$ and $p_V \geq 0.5\%$. In other words, the angle θ is meaningless in such a regime and the concurrence can be estimated on $\mathcal{C}(\rho_2^W)$. For other cases, the difference Δ_2^W increases for decreasing angle θ .

(iii) Finally, Eq. (10) can be used to establish the lower bound of $\mathcal{C}(\rho_2)$ versus p_V . Specifically, for a given value of the nonlocal fraction there exists such angle θ_0 so that the visibility $v(\theta_0, p_V) = 1$ in Eq. (10). Then, the lower bound is given by $\mathcal{C}(\rho_2) \geq \sin(2\theta_0)$ and the equality is provided by the pure state $|\theta_0\rangle_2$. The lower bound can be approximated by

$$\mathcal{C}(|\theta_0\rangle_2) = \frac{0.6784}{\sqrt{10}} p_V^{1/4} - 1.59 \times 10^{-2} p_V^{1/2} + 10^{-4} p_V. \quad (11)$$

Based on this result, one can find that the difference $\Delta_2^W < 0.164$ for an arbitrary angle θ and $0.5\% \leq p_V \leq 7\%$.

2. General two-qubit mixed states

In order to present the usefulness of our entanglement-assessment protocol for a broader range of two-qubit state ρ_{in} , we now consider two examples where we apply our protocol.

Example 1: Two-qubit GHZ symmetric mixed state (GSMS). These states represent the entire family of two-qubit mixed states with the same symmetry as the two-qubit GHZ state $|45^\circ\rangle_2$ [72]. For instance, the Werner states ρ_2^W but also the $|45^\circ\rangle_2$ state subjected to the local phase-damping or depolarizing noise [73]. The GHZ symmetric states are defined as [72]

$$\begin{aligned} \rho_2^{\text{GSMS}}(x, y) = & (\sqrt{2}y + x) |45^\circ\rangle_2 \langle 45^\circ| \\ & + (\sqrt{2}y - x) |-45^\circ\rangle_2 \langle -45^\circ| \\ & + \frac{1 - 2\sqrt{2}y}{4} \mathbb{1}_2, \end{aligned}$$

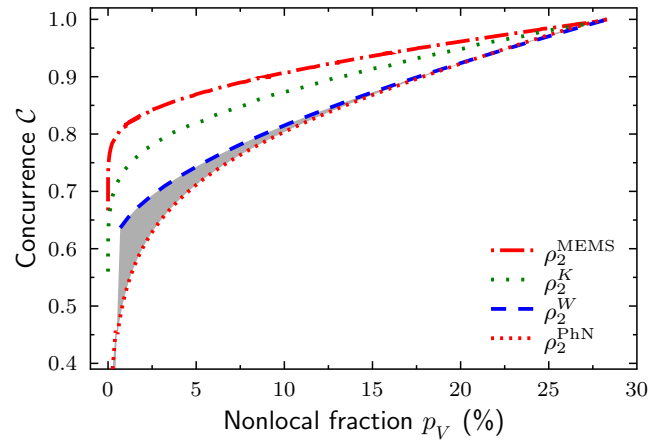


FIG. 2. The region of possible values of concurrence for given nonlocal fraction. The gray region corresponds to two-qubit GHZ symmetric mixed states and the four curves represent maximally entangled mixed states (red dash-dotted curve), Kagalwala states [75] (green dotted curve), Werner states (blue dashed curve), and two-qubit GHZ state subjected to the local phase-damping noise (red dotted curve).

where $|y| \leq (2\sqrt{2})^{-1}$ and $|x| \leq (1 + 2\sqrt{2}y)/4$. Using Eq. (1) one obtains the concurrence $\mathcal{C}(\rho_2^{\text{GSMS}}) = \max\{0, 2|x| + \sqrt{2}y - 1/2\}$.

Next, the relation between $\mathcal{C}(x, y)$ and the nonlocal fraction for 10^4 randomly generated GSMS states has been analyzed. As a result (Fig. 2), we find that the upper bound of such relation is provided by the Werner states $\rho_2^W \equiv \rho_2^{\text{GSMS}}[v/2, v/(2\sqrt{2})]$. The lower bound, on the other hand, is established by the maximally nonlocal mixed states, that is, Bell diagonal states which produce a maximal value of β_2 for given concurrence [74]. These states are given by $\rho_2^{\text{PhN}}(x) = (1 + 2x)/2 |45^\circ\rangle_2 \langle 45^\circ| + (1 - 2x)/2 |-45^\circ\rangle_2 \langle -45^\circ|$, and describe the $|45^\circ\rangle_2$ state subjected to the local phase-damping noise [73]. The relation between the concurrence and the nonlocal fraction in this case is given by $\mathcal{C}(\rho_2^{\text{PhN}}) = \mathcal{C}(|\theta_0\rangle_2)$ written in Eq. (11). Therefore, if one knows the nonlocal fraction of an arbitrary GHZ symmetric state, then its concurrence is limited by $\mathcal{C}(|\theta_0\rangle_2) \leq \mathcal{C}(\rho_2^{\text{GSMS}}) \leq \mathcal{C}(\rho_2^W)$. This limitation is of great importance if remarks (i)–(iii) are taken into account. That is, the concurrence of an arbitrary GHZ symmetric state can be determined with accuracy not greater than Δ_2^W if the measured $p_V \geq 7\%$. Note that, in general, the GSMS may denote the experimentally generated state $|45^\circ\rangle_2$ subjected to an unknown source of noise if such noise does not change the symmetry of the input state.

Example 2: Maximally entangled mixed state (MEMS). As a final example, we consider the states which maximize the value of the concurrence for a given value of the violation of the CHSH inequality [76,77]

$$\rho_2^{\text{MEMS}}(\gamma) = \gamma |45^\circ\rangle_2 \langle 45^\circ| + (1 - \gamma) |01\rangle \langle 01|,$$

where $2/3 \leq \gamma \leq 1$. Based on numerical calculation we have found that

$$\mathcal{C}(\rho_2^{\text{MEMS}}) = 1/\sqrt{2} + 0.1125/\sqrt{10} p_V^{1/4} - 9.0 \times 10^{-4} p_V^{1/2} + 2.83 \times 10^{-5} p_V.$$

As we show in Fig. 2, the concurrence $\mathcal{C}(\rho_2^{\text{MEMS}})$ exceeds $\mathcal{C}(\rho_2^W)$ in the entire range of p_V . However, the difference between these two quantities is no greater than 0.173.

Finally, our numerical calculations performed for randomly generated two-qubit mixed states ρ always satisfied the relation

$$\mathcal{C}(|\theta_0\rangle_2) \leq \mathcal{C}(\rho) \leq \mathcal{C}(\rho_2^{\text{MEMS}}), \quad (12)$$

if they reveal the same value of p_V . Therefore, we conjecture that the MEMS and pure states $|\theta\rangle_2$ provide an upper and lower limit for $\mathcal{C}(\rho)$ versus p_V for two-qubit states.

B. Quantifying genuine tripartite entanglement

1. Three-qubit werner-like states

Now we proceed to estimate the GME. We follow the same procedure as before, that is, we analyze the relationship between the GME-concurrence and nonlocal fraction. First, we concentrate on the three-qubit Werner-like states which serve as a benchmark for the robustness of multipartite entanglement [78]

$$\rho_3(\theta, v) = v |\theta\rangle_3 \langle \theta| + \frac{1-v}{8} \mathbb{1}_8, \quad (13)$$

where $|\theta\rangle_3 = \cos \theta |000\rangle + \sin \theta |111\rangle$ is the generalized GHZ state (gGHZ) and $\mathbb{1}_8$ is the 8×8 identity matrix denoting the presence of white noise. As previously, v denotes the state visibility ($0 < v \leq 1$) and we assume $0 < \theta \leq 45^\circ$. Using Eq. (3) one can find the GME concurrence as

$$\mathcal{C}_{\text{GME}}(\rho_3) = \frac{(3 \sin(2\theta) + 2)v - 2}{3}. \quad (14)$$

In order to certify the GME, we estimate the nonlocal fraction for the genuine multipartite nonlocal correlations. Such an estimation requires testing all 185 families of Bell inequalities (see [35]). As a result [Fig. 3(a)], we find that the visibility v in Eq. (13) can be approximated by p_V using

$$v(\theta, p_V) = v_3^{\text{cr}}(\theta) + g_1(\theta) p_V^{1/6} + g_2(\theta) p_V^{1/2} + g_3(\theta) p_V, \quad (15)$$

where the critical visibility $v_3^{\text{cr}}(\theta) = 1/\beta_3$ and

$$\beta_3 = \begin{cases} 1 + 0.0622\theta + 1.697\theta^2 & \text{for } 0 \leq \theta < 14.94^\circ \\ -3.391\theta^3 + 1.442\theta^4 & \text{for } 14.94^\circ \leq \theta < 29.5^\circ \\ \left(1 + 2\sqrt{1 + \sin^2(2\theta)}\right)/3 & \text{for } 29.5^\circ \leq \theta < 45^\circ \\ \sqrt{2 \sin^2(2\theta)} & \text{for } 29.5^\circ \leq \theta < 45^\circ \end{cases}$$

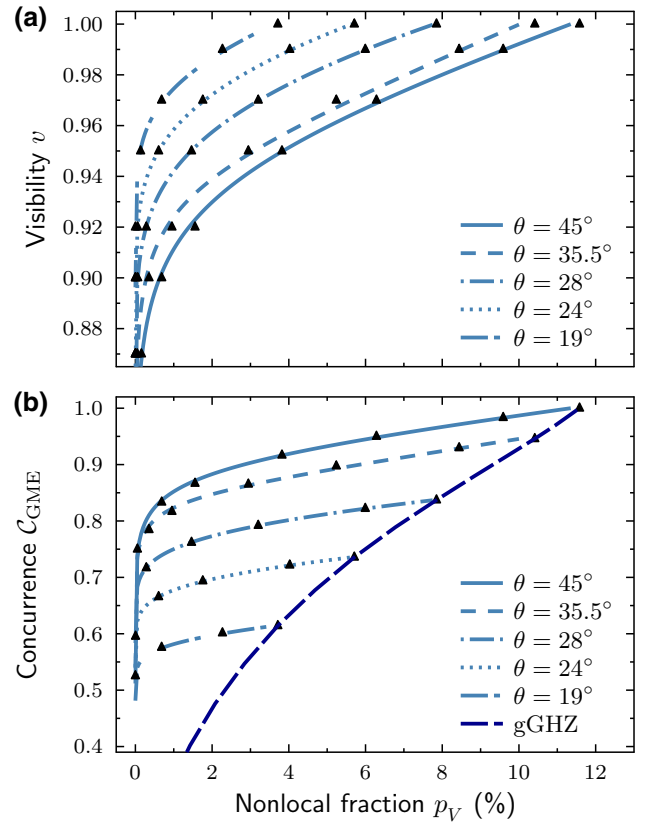


FIG. 3. (a) Visibility and nonlocal fraction for three-qubit Werner-like states given in Eq. (13). Symbols denote numerical results and solid curves correspond to their analytical approximation in Eq. (15). (b) Relation between genuine concurrence \mathcal{C}_{GME} and nonlocal fraction p_V for three-qubit Werner-like states. As previously, symbols denote numerical results whereas solid curves correspond to analytical approximation.

is the maximal strength of Bell nonlocality for three-qubit Werner-like states (see [28]). The other functions which enter Eq. (15) are given by

$$g_1(\theta) = \max\{-0.061297 + 0.55512\theta - 0.42815\theta^2, -18.58393 + 57.9917\sqrt{\theta} - 50.2727\theta + 11.209\theta^2\}/10^{1/3},$$

$$g_2(\theta) = \min\{0, 0.76306 - 4.13852\theta + 8.28077\theta^2 - 7.2943\theta^3 + 2.38884\theta^4\},$$

$$g_3(\theta) = \max\{0.0001151 - 0.0004063\theta + 0.0004321\theta^2, -0.015237 + 0.084803\theta - 0.17408\theta^2 + 0.15723\theta^3 - 0.052804\theta^4\}.$$

Based on Eqs. (14) and (15), the GME concurrence has been obtained as a function of p_V . As we see in Fig. 3(b), in contrast to $\rho_2(\theta, v)$, here the angle θ is meaningful in the entire range of attainable p_V . For instance, if one takes

$\theta_1 = 45^\circ$ (i.e., the three-qubit Werner state) and $\theta_2 = 35^\circ$, the GME concurrence is explicitly written as

$$\begin{aligned} \mathcal{C}_{\text{GME}}(\theta_1) &= 0.512 + 0.186 p_V^{1/6} - 7.1 \times 10^{-3} p_V^{1/2} \\ &\quad + 1.12 \times 10^{-4} p_V, \\ \mathcal{C}_{\text{GME}}(\theta_2) &= 0.542 + 0.155 p_V^{1/6} - 8.2 \times 10^{-3} p_V^{1/2} \\ &\quad + 1.52 \times 10^{-4} p_V. \end{aligned} \quad (16)$$

Using these equations one can easily find the difference $\Delta_3^W = \mathcal{C}_{\text{GME}}(\theta_1) - \mathcal{C}_{\text{GME}}(\theta_2)$ belongs to $(0.032, 0.048)$ when $p_V > 1\%$. Therefore, in order to establish GME concurrence $\mathcal{C}_{\text{GME}}(\rho_3)$, we need to evaluate not only the value of p_V but also the underlying angle θ . Without prior knowledge of the angle θ , its value can be determined from the distribution of the strength of violation for random measurements (Appendix B). This requires the accumulation of data on the strength of violation of local realism for a sequence of randomly chosen measurements. In a typical experimental investigation of p_V [32,35,64], such a set is known without any additional effort and, hence, one can establish the value of GME concurrence.

On the other hand, by inserting $v(\theta, p_V) = 1$ into Eq. (15) one can derive the GME concurrence for pure states $|\theta\rangle_3$. It can be approximated by [35]

$$\mathcal{C}_{\text{GME}}(|\theta\rangle_3) = \left(0.068 p_V + 0.06 p_V^{1/2}\right)^{1/2}, \quad (17)$$

which denotes the lower bound of $\mathcal{C}_{\text{GME}}(\rho_3)$ with given p_V .

2. Other examples of states

We note that the general analysis of the three-qubit mixed states is beyond the scope of the paper, as there is no general analytical formula of the genuine concurrence. Therefore, we examine a few examples which illustrate the usefulness of our approach.

Example 3: Three-qubit GHZ symmetric mixed state (GSMS). A natural extension of the three-qubit Werner-like states is the family of GHZ symmetric states. In the three-qubit case, they are given by

$$\begin{aligned} \rho_3^{\text{GSMS}}(x, y) &= \left(\frac{2\sqrt{3}}{3}y + x\right) |45^\circ\rangle_3 \langle 45^\circ| \\ &\quad + \left(\frac{2\sqrt{3}}{3}y - x\right) |-45^\circ\rangle_3 \langle -45^\circ| \\ &\quad + \frac{3 - 4\sqrt{3}y}{24} \mathbb{1}_8, \end{aligned} \quad (18)$$

where $-1/(4\sqrt{3}) \leq y \leq \sqrt{3}/4$, $|x| \leq (1 + 4\sqrt{3}y)/8$ and the GME concurrence $\mathcal{C}_{\text{GME}}(\rho_3^{\text{GSMS}}) = \max\{0, 2|x| + \sqrt{3}y - 3/4\}$.

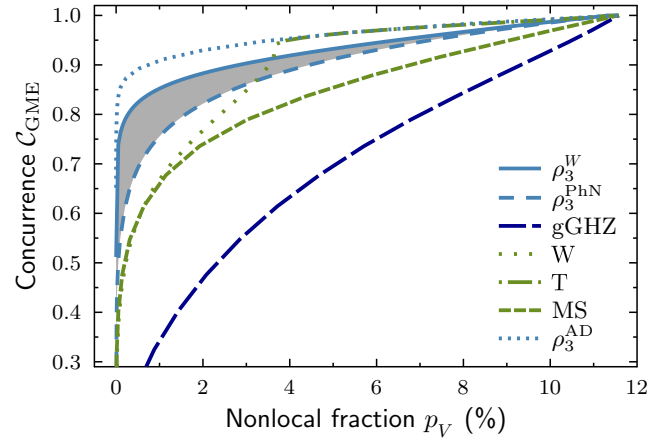


FIG. 4. The region of possible values of genuine concurrence for given nonlocal fraction. The gray region corresponds to three-qubit GHZ symmetric mixed states and the four blue curves represent Werner states (solid curve), three-qubit GHZ state subjected to the local phase-damping noise (short dashed curve), three-qubit GHZ state subjected to the local amplitude-damping noise (dotted curve), and generalized GHZ states (blue dashed curve). Furthermore, the three green curves show the tetrahedral states (dot-dashed curve), generalized W states (dotted curve), and maximal slice states (short dashed curve).

For these states, similar remarks can be drawn as in Example 1. Specifically, the upper bound of the GME concurrence for a given value of p_V is provided by the three-qubit Werner state ρ_3^W (Fig. 4). The lower bound is observed for $\rho_3^{\text{PhN}}(x) = (\frac{1}{2} + x) |45^\circ\rangle_3 \langle 45^\circ| + (\frac{1}{2} - x) |-45^\circ\rangle_3 \langle -45^\circ|$, that is, the GHZ state subjected to the local phase-damping noise [73]. The GME concurrence is approximated by

$$\mathcal{C}_{\text{GME}}(\rho_3^{\text{PhN}}) = 0.4012 p_V^{1/6} - 0.0118 p_V^{1/2} + 9.0 \times 10^{-5} p_V,$$

and, hence, the difference $\Delta_3^W \leq 0.14$. Interestingly, results obtained for ρ_3^{PhN} are significantly different with respect to those of $|\theta\rangle_3$, as opposed to the case of two-qubit states. In summary, for all ρ_3^{GSMS} states, the following relation is observed

$$\mathcal{C}_{\text{GME}}(|\theta\rangle_3) < \mathcal{C}_{\text{GME}}(\rho_3^{\text{PhN}}) \leq \mathcal{C}_{\text{GME}}(\rho_3^{\text{GSMS}}) \leq \mathcal{C}_{\text{GME}}(\rho_3^W),$$

where we assume that each state reveals the same value of the nonlocal fraction.

Example 4: GHZ state under the amplitude-damping noise. Let us recall that the GHZ-symmetric states describe two basic examples of the noisy GHZ state, that is, affected by local phase-damping and depolarizing noise. Here we investigate another important example, namely the GHZ state subjected to the local amplitude-damping

(AD) noise [73]

$$\rho_3^{\text{AD}}(\alpha) = \sum_{i,j,k=1}^2 \mathcal{K}_{i,j,k}(\alpha) |45^\circ\rangle_3 \langle 45^\circ| \mathcal{K}_{i,j,k}^\dagger(\alpha), \quad (19)$$

where $\mathcal{K}_{i,j,k}(\alpha) = \mathcal{K}_i(\alpha) \otimes \mathcal{K}_j(\alpha) \otimes \mathcal{K}_k(\alpha)$ denotes the tensor product of the appropriate Kraus operators [73] and $0 \leq \alpha \leq 1$. Our calculations reveal that the genuine concurrence $\mathcal{C}_{\text{GME}}(\rho_3^{\text{AD}}) \geq \mathcal{C}_{\text{GME}}(\rho_3^{\text{W}})$ in the entire range of p_V (Fig. 4). Furthermore, the calculation has been repeated for the bit flip noise, providing results slightly smaller than those of the Werner states. This means that if the GHZ state is transmitted via one of the basic quantum channels (unknown in principle), then the genuine concurrence of the output state is greater than or equal to that of ρ_3^{PhN} .

Example 5: Three-qubit pure states. Finally, we analyze the relationship between the genuine concurrence and the nonlocal fraction for other examples of three-qubit pure state that are important for quantum communication protocols [79], namely the tetrahedral (T) states [60,80], the generalized W states [81], and the maximal slice (MS) states [82]

$$\begin{aligned} |\psi_{\text{T}}\rangle &= t_0 (|001\rangle + |010\rangle + |100\rangle) + \sqrt{1 - 3t_0^2} |111\rangle, \\ |\psi_{\text{W}}\rangle &= \frac{w_0}{\sqrt{2}} (|001\rangle + |010\rangle) + w_1 |100\rangle, \\ |\psi_{\text{MS}}\rangle &= \frac{1}{\sqrt{2}} (|000\rangle + m_0 |110\rangle + m_1 |111\rangle), \end{aligned} \quad (20)$$

where the standard normalization condition is assumed. As we show in Fig. 4, in all these cases the relationship between the genuine concurrence and the nonlocal fraction satisfy the relation

$$\mathcal{C}_{\text{GME}}(|\theta\rangle_3) < \mathcal{C}_{\text{GME}}(|\psi_{\text{T,W,MS}}\rangle) \leq \mathcal{C}_{\text{GME}}(\rho_3^{\text{AD}}).$$

In other words, if one assumes that the state under the question remains unknown, then its genuine concurrence can be estimated from the bottom using $\mathcal{C}_{\text{GME}}(|\theta\rangle_3)$.

IV. EXPERIMENTAL IMPLEMENTATION

A. Experimental setup

We have constructed the experimental setup depicted in Fig. 5 to produce and characterize three-qubit states. Our experiment is implemented on the platform of linear optics and it encodes qubits into spatial and polarization states of single photons. The setup utilizes entangled photon pairs generated using Type-I parametric down-conversion in a β -BBO crystal cascade (referred to as Kwiat source [83]) at $\lambda = 710$ nm. A laser beam of a wavelength of $\lambda = 355$ nm pumps two identically cut nonlinear crystals, with optical axis in mutually perpendicular

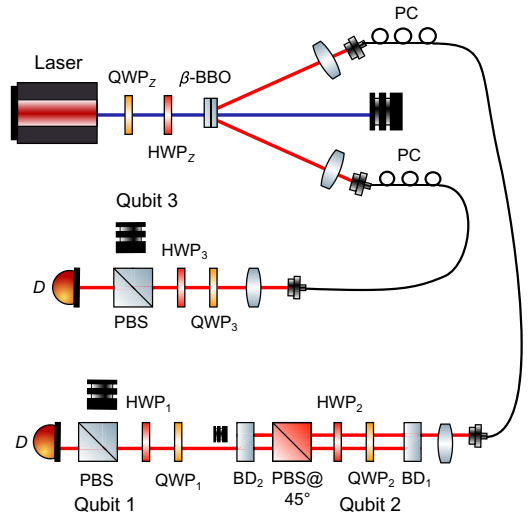


FIG. 5. Experimental setup. Legend: PBS, polarization beam splitter; BD, beam displacer; PC, polarization controller; β -BBO, nonlinear crystal β -barium borate; D, detector; HWP, half-wave plate; QWP, quarter wave plate.

planes defining horizontal and vertical basis. If pumped by horizontally (vertically) polarized pump beam, pairs of vertically (horizontally) polarized photons are generated. By setting half-wave plate HWP_Z at angle $\frac{\theta}{2}$ both crystals are coherently pumped and generate photons in a state of the form of

$$\cos \theta |HH\rangle + \sin \theta |VV\rangle. \quad (21)$$

The first (second) position in the ket denotes polarization of the first (second) photon. The probability of generating two pairs simultaneously is negligible.

In order to generate the three-qubit states, we incorporate spatial mode encoding to be used in addition to polarization encoding. For this purpose, the first photon is subjected to the beam displacer (BD_1). Here BD_1 deviates vertically polarized photons upwards whereas horizontally polarized photons continue straightforward. Therefore, one can denote by $|0\rangle$ ($|1\rangle$) spatial mode of photons in the upper (lower) arm. At the same time by associating H (V) polarization with logical states $|0\rangle$ ($|1\rangle$) one can immediately identify that by the action of BD_1 the original two-qubit state (21) becomes a generalized GHZ state in its canonical form

$$|\theta\rangle_3 = \cos \theta |000\rangle + \sin \theta |111\rangle. \quad (22)$$

Here the first qubit in the ket denotes first photon's spatial mode and second (third) qubit denotes the first (second) photon's polarization state.

Having the desired state prepared, all three qubits are subjected to local projections (hereafter, $|\hat{\Pi}_1 \otimes \hat{\Pi}_2 \otimes \hat{\Pi}_3\rangle$). The third qubit is projected simply by using a combination

of quarter and half wave plates (QWP₃ and HWP₃) accompanied by a polarizing beam splitter (PBS). The remaining two qubits are encoded into the spatial and polarization state of the first photon. Using a similar sequence (QWP₂, HWP₂, and PBS) spreading over both spatial modes of this photon, we achieve projection of the second qubit. At this stage, a BD₂ is used to convert the spatial encoding of the first qubit to polarization encoding. Once polarizationally encoded, the sequence of QWP₁, HWP₁, and PBS is used to perform the first qubit's projection. At the end of the setup, both photons are led to single-photon detectors and the rate of coincident detections is measured for every projection setting.

For the purposes of this experiment, we require the setup to prepare and characterize all pure computational basis states, that is, $|\text{basis}\rangle = \{|000\rangle, |001\rangle, \dots, |111\rangle\}$. This is simply achieved by setting $\theta = 0^\circ$ resulting in generation of the $|000\rangle$ state and imposing single-qubit NOT gates in the modes where the qubit is required in the $|1\rangle$ state. These NOT gates are implemented by adding a 45° bias to the HWP associated with this qubit. All these states were later used to synthesize white noise. Then, various quasi-pure GHZ states were also prepared. All experimental data accumulated in this experiment are available in the Supplemental Material [84].

The experiment is carried out in three steps. First, we generate the desired gGHZ states and verify their quality using standard state tomography (Sec. IV B). For such verification, it is necessary to align the reference frame. Having the reconstructed density matrix, one can estimate experimental imperfections and also test the concept of nonlocal fraction by simulating 10^8 random projections imposed to this matrix. The second experimental step is the truly RFI scenario involving 8000 random projections directly imposed to the generated photons. This constitutes the main result of our paper (Sec. IV C). Finally, in Sec. IV D, we also perform experimental estimation of GME-concurrence measurement on arbitrarily mixed Werner states by adding white noise as explained previously.

B. Nonlocal fraction measurements: aligned reference frames

First, we consider a scenario when the observers share common reference frames. The experimental setup has been adjusted in such a way to generate the gGHZ states, $|\theta\rangle_3$, for two different angles accounting for 35° and 45° . Note that the latter case denotes the prototype GHZ state. For each adjustment of θ , the output-state density matrix, $\rho_\theta^{\text{expt}} \equiv \rho_3^{\text{expt}}(\theta)$, is reconstructed by evaluating the quantum state tomography and maximum-likelihood estimation [85,86]. An exemplary result is shown in Fig. 6. Then, we determine the fidelity F of $\rho_\theta^{\text{expt}}$ with respect to the ideal pure state $|\theta\rangle_3$, $F(\rho_\theta^{\text{expt}}) = \text{Tr}(\rho_\theta^{\text{expt}}|\theta\rangle_3\langle\theta|)$. As a result, we find that $F(\rho_\theta^{\text{expt}})$ is always greater than 0.980 ± 0.002 for

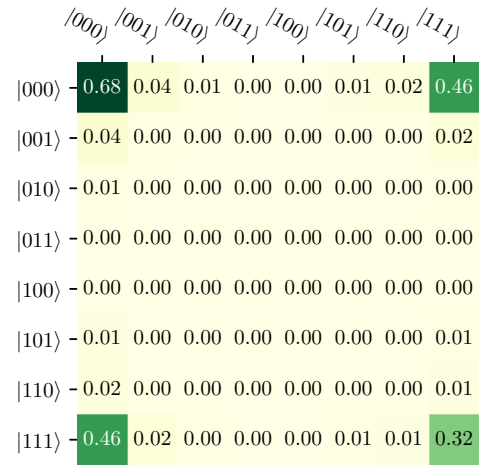


FIG. 6. Visualization of the real part of the density matrix $\rho^{\text{expt}} \theta = 35^\circ$. All values of the imaginary part of ρ^{expt} are less than 0.025.

all values of θ confirming the good quality of our source. The uncertainty of the fidelity has been determined by Monte Carlo simulations of Poissonian noise distribution.

The fact that $F(\rho_\theta^{\text{expt}}) < 1$ is naturally caused by the presence of experimental imperfections such as the improper setting of individual components or depolarization effects. Consequently, an effective form of the generated state should be considered as the three-qubit Werner-like state $\rho_3(\theta, v_\theta)$ in Eq. (13), where v_θ is associated with the strength of the effective noise inherently present during the experiment. The presence of such noise is certified by a reduction in purity, $P(\rho) = \text{Tr}(\rho^2)$, of the output state. By straightforward calculations we have found that $P(\rho_{35^\circ}^{\text{expt}}) = 0.982 \pm 0.005$ and $P(\rho_{45^\circ}^{\text{expt}}) = 0.976 \pm 0.005$. Then, using the relation $P(\rho) = \frac{1+7v_0^2}{8}$ [87] the visibility v_0 has been estimated. In our case the visibility is equal to $v_{35^\circ} = 0.990 \pm 0.003$ and $v_{45^\circ} = 0.986 \pm 0.003$. These values are further utilized to establish an appropriate reference point of theoretical predictions.

Next, using the reconstructed output state, $\rho_\theta^{\text{expt}}$, and numerical procedure described in Sec. II B, the nonlocal fraction has been evaluated

$$\begin{aligned} p_V(\rho_{45^\circ}^{\text{expt}}) &= 9.0 \pm 0.9\%, \\ p_V(\rho_{35^\circ}^{\text{expt}}) &= 8.2 \pm 0.7\%. \end{aligned} \quad (23)$$

For each state, 10^8 different settings have been examined numerically. Although the density matrix was obtained via tomography in an aligned reference frame scenario, processing of probabilities corresponding to these random projection settings is identical to the RFI situation. Comparing these results with theoretical prediction, $p_V(45^\circ, v_{45^\circ}) = 8.830\%$ and $p_V(35^\circ, v_{35^\circ}) = 8.279\%$, we see a very good agreement between both sets of outcomes.

C. Nonlocal fraction measurements: reference frames independent approach

In the second step, we relax the experimental requirements and consider the reference-frame-independent approach. In this case, all three qubits of the desired $\rho_\theta^{\text{expt}}$ state are subjected to randomly chosen local projections $|\hat{\Pi}_1 \otimes \hat{\Pi}_2 \otimes \hat{\Pi}_3\rangle$. Note that, by the definition of the nonlocal fraction, their actual value is not important and, so, there is no need to calibrate the experimental devices. The whole process includes $n = 8000$ projection settings. For each adjustment of θ and $|\hat{\Pi}_1 \otimes \hat{\Pi}_2 \otimes \hat{\Pi}_3\rangle$, we measure coincidence detections (CC) over approximately 20 s and we registered one value of CC per projection. The values of CC are used to determine all correlation coefficient (see [35,87]) and, then, to test all 185 Bell inequalities relevant for the genuine multipartite nonlocal correlations [56]. Note that in this test all possible relabeling of parties, inputs, and outputs has been taken into account. The value of the Bell inequality is determined with precision ± 0.015 . Dividing the number of projection setting which provide violation of local realism by the total number of setting n , the nonlocal fraction has been estimated. We obtain the following results:

$$\begin{aligned} p_V^{\text{CC}}(45^\circ) &= 8.6 \pm 1.6\%, \\ p_V^{\text{CC}}(35^\circ) &= 8.7 \pm 1.2\%. \end{aligned} \quad (24)$$

As we show in Fig. 7, our results in Eq. (24) match correctly to the attainable range of theoretical predictions if the precision of v_0 is included. Specifically, for the error bar of v_0 equal to ± 0.003 , one obtains $8.302\% \leq p_V(45^\circ, v_{45^\circ}) \leq 9.377\%$ and $7.735\% \leq p_V(35^\circ, v_{35^\circ}) \leq 8.848\%$. However, the values of $p_V^{\text{CC}}(\theta)$

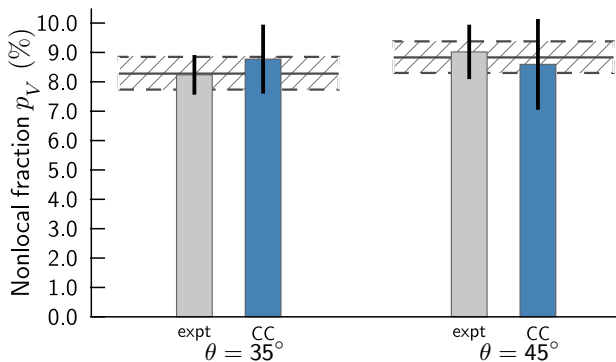


FIG. 7. Comparison of the nonlocal fraction estimated for the reconstructed density matrix $p_V(\rho_\theta^{\text{expt}})$ (gray bar) and measured coincidence detections $p_V^{\text{CC}}(\theta)$ (blue bar) for angle $\theta = 35^\circ, 45^\circ$. Horizontal hatched areas show theoretical predictions, solid lines correspond to $p_V(\theta, v_\theta)$, and dashed lines denote $p_V(\theta, v_\theta \pm 0.03)$.

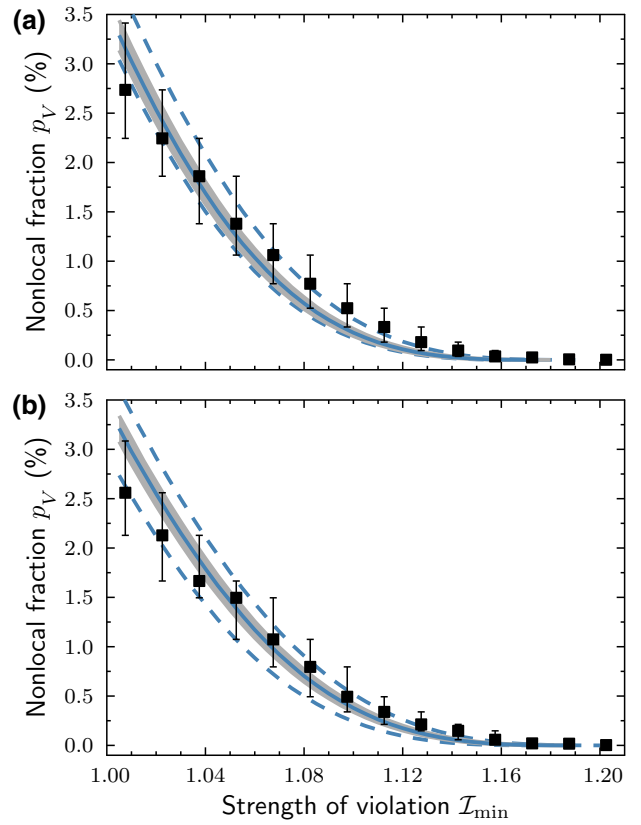


FIG. 8. Distribution of the strength of violation for randomly sampled measurements for (a) $\theta = 35^\circ$ and (b) $\theta = 45^\circ$. In both panels, symbols denote experimental results whereas gray areas depict theoretical predictions for $\rho_3(\theta, v_\theta \pm 0.003)$. Dashed lines correspond to theoretical calculations for (a) $\rho_3(35^\circ, 1)$ and $\rho_3(35^\circ, 0.985)$ and (b) $\rho_3(45^\circ, 0.990)$ and $\rho_3(45^\circ, 0.975)$.

slightly differ from $p_V(\rho_\theta^{\text{expt}})$ in Eq. (23). In particular, $p_V^{\text{CC}}(45^\circ) < p_V^{\text{CC}}(35^\circ)$. To explain such difference, we emphasize that owing to inherent experimental fluctuation, the generated state slightly varies over the course of the entire data acquisition time (about two days). For that reason, one may expect some fluctuations of the inherent noise arising due to, for example, dephasing and depolarization.

In order to verify this conclusion, the distribution of the strength of violation for random measurements has been analyzed. In other words, we simulate a robustness of the nonlocal fraction p_V^{CC} using the accumulated data for random sampling. As we see in Fig. 8, for both values of angle θ the simulated relationship between p_V^{CC} and \mathcal{I}_{\min} has a similar shape as its theoretical counterpart (see Appendix B). Furthermore, by fitting our experimental data with Eq. (B3) we have found the following results $\{\theta, v_{45^\circ}\} \approx \{44.7^\circ, 0.984\}$ and $\{\theta, v_{35^\circ}\} \approx \{36.0^\circ, 0.996\}$, which is in line with our previous observations. Note that these fitted values are sufficient to establish the GME

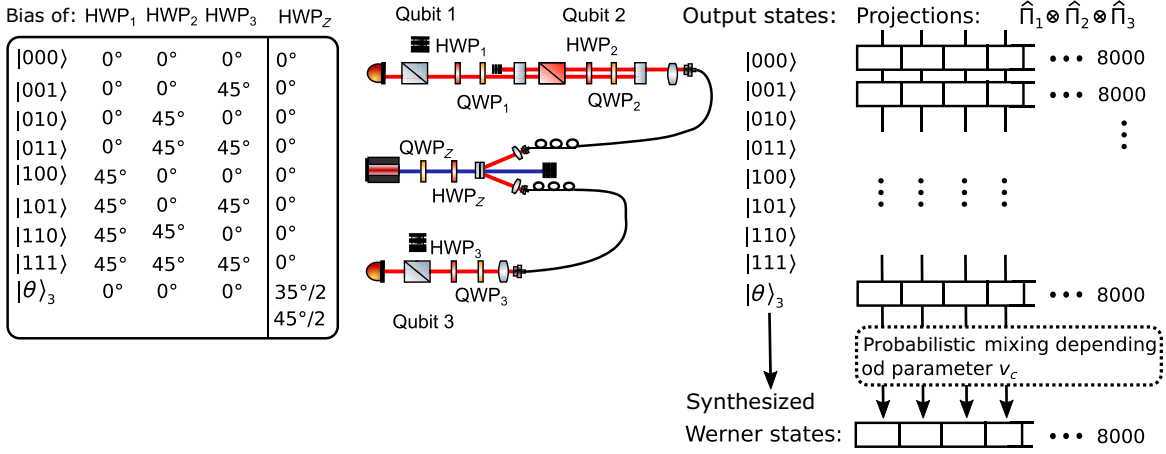


FIG. 9. Scheme of the synthesizing procedure for all 8000 random projections $|\hat{\Pi}_1 \otimes \hat{\Pi}_2 \otimes \hat{\Pi}_3\rangle$. On the left-hand side of this scheme we provide HWP settings for each three-qubit state. The final state $\hat{\rho}_W$ is mixed according to a prescription given in Eq. (25).

concurrence using Eq. (14) without prior knowledge about the generated state.

D. Genuine concurrence measure: reference-frame-independent approach

The final stage of our experiment is to measure the GME concurrence for the Werner-like states. In order to do that, the Werner-like states $\rho_3^{\text{expt}}(\theta, v)$ were synthesized with controlled visibility v in the range $[0.9; v_\theta]$. This is accomplished by controlled mixing (with probability v_c) the output state $\rho_\theta^{\text{expt}}$ and white noise, that is, $v_c \rho_\theta^{\text{expt}} + (1 - v_c) \rho_{\text{white noise}}$. As a result, one has

$$\rho_3^{\text{expt}}(\theta, v) = v_c v_\theta |\theta\rangle_3 \langle \theta| + \sum_{\text{basis}} \frac{1 - v_c v_\theta}{8} |\text{basis}\rangle \langle \text{basis}|, \quad (25)$$

where the total visibility $v \equiv v_c v_\theta$ with v_θ being a constant value defined above and controlled parameter v_c varying with a step $\delta_v = 0.01$.

Now, to synthesize projection results CC for any mixed state in Eq. (25), the experimental setup was set to gradually generate eight basis states $|\text{basis}\rangle$. Similarly as in Sec. IV C, each of the states is subjected to the same set of random projections $|\hat{\Pi}_1 \otimes \hat{\Pi}_2 \otimes \hat{\Pi}_3\rangle$ as those of ρ^{expt} (including tomography projections). Finally, values of CC are probabilistically mixed according to the following routine (Fig. 9)

$$CC_i(\theta, v) = v_c CC_i(\rho_\theta^{\text{expt}}) + \sum_{\text{basis}} \frac{1 - v_c}{8} CC_i(|\text{basis}\rangle), \quad (26)$$

where $CC_i(\theta, v) \equiv CC_i[\rho_3^{\text{expt}}(\theta, v)]$ and $CC_i(\rho)$ denotes the values of CC for the state ρ and the i th projector

$|\hat{\Pi}_1^{(i)} \otimes \hat{\Pi}_2^{(i)} \otimes \hat{\Pi}_3^{(i)}\rangle$. This procedure results in 8000 values of CC for each generated state $\rho_3^{\text{expt}}(\theta, v)$ that can be further analyzed. Note that for every state, all CC_i are normalized with respect to the overall generation rate for the particular state.

Based on these results, the nonlocal fraction of $\rho_3^{\text{expt}}(\theta, v)$ has been determined. As we see in Fig. 10(a), our measurements are in good agreement with theoretical predictions given in Eq. (15). Finally, using Eq. (16) the GME concurrence for the Werner-like states has been established and the accomplished results are in perfect agreement with theory [Fig. 10(b)]. Specifically, for the exemplary states discussed in previous subsections, we obtain

$$\begin{aligned} \mathcal{C}_{\text{GME}}(45^\circ) &= 0.97 \pm 0.01, \\ \mathcal{C}_{\text{GME}}(35^\circ) &= 0.93 \pm 0.01, \end{aligned} \quad (27)$$

whereas theoretical predictions yield $\mathcal{C}_{\text{GME}}(45^\circ, v_{45^\circ}) = 0.977$ and $\mathcal{C}_{\text{GME}}(45^\circ, v_{45^\circ}) = 0.924$.

V. CONCLUSIONS

In conclusion, we have theoretically and experimentally investigated the entanglement-assessment protocol for two- and three-qubit Werner-like states. Our proposal is based on the concept of the nonlocal fraction which denotes the probability of detection of nonlocal correlation under randomly measurements. Using numerical calculations, we have found the relationship between the degree of entanglement and nonlocal fraction. Then, our method has been successfully applied to the experimental measurements of the GME concurrence of the three-qubit Werner-like state, revealing perfect agreement with theoretical predictions.

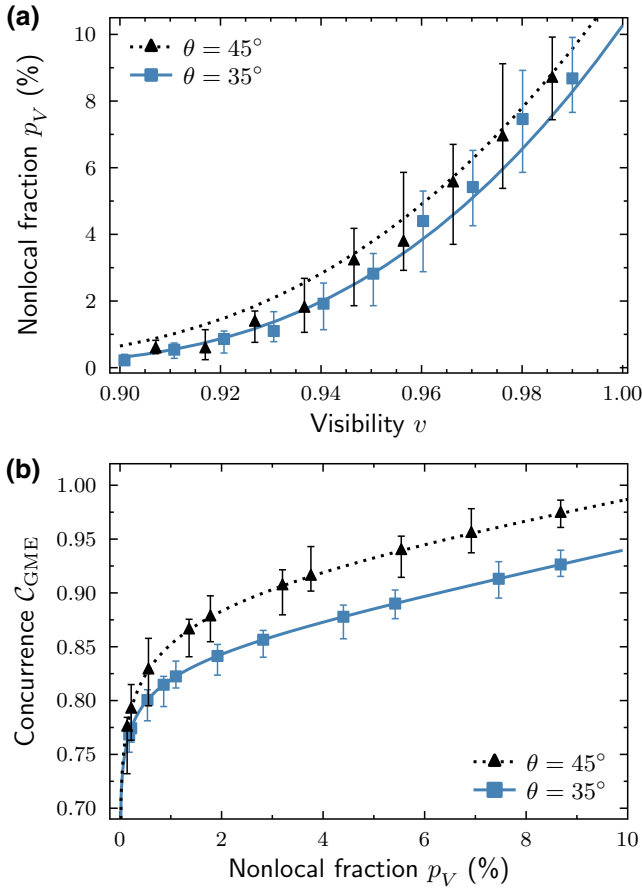


FIG. 10. (a) Dependence of the nonlocal fraction on the visibility and (b) the relation between genuine concurrence and nonlocal fraction for three-qubit Werner-like states. In both panels, symbols denote experimental measurements for $\theta = 35^\circ$ (triangles) and $\theta = 45^\circ$ (squares) whereas curves depict theoretical predictions.

The advantage of using random sampling in our protocol is a great simplification of experimental procedures as the alignment and calibration of remote devices are no longer necessary. Therefore, our protocol can be applied in an unstable environment, where the previously mentioned requirements are hard to meet.

Although in this paper we focus on the Werner-like states, our protocol can also be used for an arbitrary mixed state. In this broader context, the protocol can operate as an indicator of a lower bound of entanglement for the state under considerations. From the point of view of quantum communications, such finding is of great importance as it allows the characterization of a minimal efficiency on the communication protocol. One should also emphasize that Werner states are considered as the paradigmatic examples of experimental noise. This fact justifies the choice of Werner-like states as a test bed for our protocol.

ACKNOWLEDGMENTS

The authors thank Cesnet for providing data management services. Numerical calculations were performed in the Wrocław Centre for Networking and Supercomputing, Poland. K.J., A.B., A.Č., and K.L. acknowledge financial support by the Czech Science Foundation under the project No. 20-17765S. The authors also acknowledge project CZ.02.1.01/0.0/0.0/16_019/0000754 of the Ministry of Education, Youth, and Sports of the Czech Republic. K.J. also acknowledges the Palacký University internal grant No. IGA-PrF-2021-004.

APPENDIX A: ANALYTICAL DERIVATION OF Eq. (9)

The CHSH inequality for general two-qubit state ρ can be written as [88]

$$|\vec{a}_0 \cdot R^\rho \cdot (\vec{b}_0 + \vec{b}_1) + \vec{a}_1 \cdot R^\rho \cdot (\vec{b}_0 - \vec{b}_1)| \leq 2, \quad (\text{A1})$$

where $\vec{a}_0, \vec{a}_1, \vec{b}_0,$ and \vec{b}_1 are unitary vectors in \mathbb{R}^3 and R^ρ denotes the 3×3 correlation matrix with elements $R_{ij}^\rho = \text{Tr}[\rho (\sigma_i \otimes \sigma_j)]$ given in terms of the three Pauli matrices. For the special case, when ρ stands for the Werner state (in the form proposed in Ref. [69]), the correlation matrix $R = -v\mathbb{1}_3$, where v is the visibility.

Next we introduce a pair of unitary vectors \vec{c}_0 and \vec{c}_1 by $\vec{b}_0 + \vec{b}_1 = \vec{c}_0\sqrt{2(1+x)}$, $\vec{b}_0 - \vec{b}_1 = \vec{c}_1\sqrt{2(1-x)}$, where $x = \vec{b}_0 \cdot \vec{b}_1$. Substituting all these quantities into Eq. (A1), one has

$$|\vec{a}_0 \cdot \vec{c}_0\sqrt{1+x} + \vec{a}_1 \cdot \vec{c}_1\sqrt{1-x}| \leq \frac{\sqrt{2}}{v}. \quad (\text{A2})$$

To prove Eq. (9) we shall find how often inequality (A2) is violated when unit vectors $\vec{a}_0, \vec{a}_1, \vec{c}_0, \vec{c}_1$ and the variable x are chosen independently, randomly, and isotropically. Following arguments presented in Ref. [34], to solve the above problem, it is sufficient to sample x and dot products $\vec{a}_0 \cdot \vec{c}_0$ and $\vec{a}_1 \cdot \vec{c}_1$ uniformly from the interval $[-1, 1]$ as the actual direction of individual vectors is irrelevant (hereafter, we use $\alpha = \vec{a}_0 \cdot \vec{c}_0$ and $\beta = \vec{a}_1 \cdot \vec{c}_1$).

From a geometrical point of view, this solution denotes the fraction of the cube's volume containing points (α, β, x) violating the inequality (A2). For a particular fixed x , the regime of the cube containing points violating Eq. (A2) are given by

$$\beta > \frac{\sqrt{2} - \alpha v \sqrt{1+x}}{v \sqrt{1-x}},$$

$$\beta < -\frac{\sqrt{2} + \alpha v \sqrt{1+x}}{v \sqrt{1-x}}. \quad (\text{A3})$$

Therefore, with some straightforward calculation, one can find that the fraction of Alice and Bob's measurement

directions that would violate the CHSH inequality and, hence, the nonlocal fraction is given by

$$p_V = 4 \int_{x_-}^{x_+} \frac{(\sqrt{2} - v(\sqrt{1-x} + \sqrt{1+x}))^2}{V_{\text{cube}} v^2 \sqrt{1-x^2}} dx, \quad (\text{A4})$$

where $V_{\text{cube}} = 2^3$ denotes the volume of the cube, the integration is performed for $x_{\pm} = \pm\sqrt{(2v^2-1)/v^4}$ and the result is multiplied by four to take into account any possible relabeling of measurement settings and/or outcomes. This is because, for any given measurement directions, at most one of the CHSH inequalities can be violated. The value of x_{\pm} is caused by the fact that for fixed v and $x > x_+$ ($x < x_-$), there are no pairs (α, β) (both in the interval $[-1, 1]$) which satisfy constraints (A2). After appropriate integration in Eq. (A3), we obtain Eq. (9). Note that for $v = 1$ the nonlocal fraction $p_V = 2(\pi - 3)$, which is in line with [34].

APPENDIX B: NONLOCAL FRACTION BASED ON THE DISTRIBUTION OF THE STRENGTH OF VIOLATION

Let us take a three-qubit state ρ and a finite set of measurement settings $\{M_i\}$, where $i = 1, \dots, m$. To verify whether the genuine nonlocal correlations are generated for the state ρ and given measurement setting \hat{M}_i , one should test 185 Bell inequalities [56] of the form $\tilde{\mathcal{I}}_j(\rho|M_i) \leq C_j^{\text{LHV}}$, where $j = 1, \dots, 185$. To this end, it is expedient to consider $C_j^{\text{LHV}} = 1$ and $\mathcal{I}_j(\rho|M_i) = \tilde{\mathcal{I}}_j(\rho|M_i)/C_{\text{LHV}}$. Based on such a test, a maximal strength of violation for \hat{M}_i is determined as $\mathcal{I}_i^{\text{max}}(\rho) = \max_j \{\mathcal{I}_j(\rho|M_i)\}$, where the maximum is taken over 185 Bell inequalities. Dividing the number of $\mathcal{I}_i^{\text{max}}(\rho)$, satisfying the constraints $\mathcal{I}_i^{\text{max}}(\rho) > 1$, by the number of measurement settings m , the nonlocal fraction is estimated as

$$p_V(\rho) = \lim_{m \rightarrow \infty} \frac{n(\{\mathcal{I}_i^{\text{max}}(\rho), \mathcal{I}_i^{\text{max}}(\rho) > 1\})}{m}. \quad (\text{B1})$$

Next, let us consider a state $\sigma(v) = v\rho + (1-v)/8 \cdot \mathbb{1}_8$, that is, a statistical mixture of the state ρ and white noise. Then, one can easily prove that $\mathcal{I}_j(\sigma|M_i) = v\mathcal{I}_j(\rho|M_i)$ and, hence, the maximal strength of violation $\mathcal{I}_i^{\text{max}}(\sigma) = v\mathcal{I}_i^{\text{max}}(\rho)$. Consequently, by analogy to Eq. (B1), the nonlocal fraction of state σ can be written as

$$p_V(\sigma) = \lim_{m \rightarrow \infty} \frac{n(\{\mathcal{I}_i^{\text{max}}(\rho), \mathcal{I}_i^{\text{max}}(\rho) > \mathcal{I}_{\text{min}} = 1/v\})}{m}. \quad (\text{B2})$$

In other words, if one knows the distribution of the strength of violation $\{\mathcal{I}_i^{\text{max}}(\rho)\}$, then the nonlocal fraction of any

state $\sigma(v)$ can be estimated by suitable shiftiness of the classical threshold denoted by \mathcal{I}_{min} . As a result, one can find a relationship between $p_V(\sigma)$ and the visibility v [cf. Fig. 3(a)].

In particular, if we assume that $\rho = \rho_3(\theta, v_0)$, then the state $\sigma(v) = v \cdot v_0 |\theta\rangle_3 \langle \theta| + (1-v \cdot v_0)/8 \cdot \mathbb{1}_8$ and the relationship between $p_V(\sigma)$ and v is described by Eq. (15) with unknown values v_0 and angle θ . Therefore, Eq. (15) can be rewritten as

$$v = \frac{1}{v_0} \left(v_3^{\text{cr}}(\theta) + g_1(\theta) p_V^{1/6} + g_2(\theta) p_V^{1/2} + g_3(\theta) p_V \right). \quad (\text{B3})$$

By fitting the distribution $p_V(\sigma)$ versus v described previously with Eq. (B3) one obtains an approximation of both parameters v_0 and θ .

-
- [1] Q.-C. Sun, Y.-L. Mao, S.-J. Chen, W. Zhang, Y.-F. Jiang, Y.-B. Zhang, W.-J. Zhang, S. Miki, T. Yamashita, H. Terai, X. Jiang, T.-Y. Chen, L.-X. You, X.-F. Chen, Z. Wang, J.-Y. Fan, Q. Zhang, and J.-W. Pan, Quantum teleportation with independent sources and prior entanglement distribution over a network, *Nat. Photon* **10**, 671 (2016).
 - [2] R. Valivarthi, M. G. Puigibert, Q. Zhou, G. H. Aguilar, V. B. Verma, F. Marsili, M. D. Shaw, S. W. Nam, D. Oblak, and W. Tittel, Quantum teleportation across a metropolitan fibre network, *Nat. Photon* **10**, 676 (2016).
 - [3] R. Ursin, F. Tiefenbacher, T. Schmitt-Manderbach, H. Weier, T. Scheidl, M. Lindenthal, B. Blauensteiner, T. Jennewein, J. Perdigues, P. Trojek, B. Ömer, M. Fürst, M. Meyenburg, J. Rarity, Z. Sodnik, C. Barbieri, H. Weinfurter, and A. Zeilinger, Entanglement-based quantum communication over 144 km, *Nat. Phys.* **3**, 481 (2007).
 - [4] J. Yin, J.-G. Ren, H. Lu, Y. Cao, H.-L. Yong, Y.-P. Wu, C. Liu, S.-K. Liao, F. Zhou, Y. Jiang, X.-D. Cai, P. Xu, G.-S. Pan, J.-J. Jia, Y.-M. Huang, H. Yin, J.-Y. Wang, Y.-A. Chen, C.-Z. Peng, and J.-W. Pan, Quantum teleportation and entanglement distribution over 100-kilometre free-space channels, *Nature* **488**, 185 (2012).
 - [5] X.-S. Ma, T. Herbst, T. Scheidl, D. Wang, S. Kropatschek, W. Naylor, B. Wittmann, A. Mech, J. Kofler, E. Anisimova, V. Makarov, T. Jennewein, R. Ursin, and A. Zeilinger, Quantum teleportation over 143 kilometres using active feed-forward, *Nature* **489**, 269 (2012).
 - [6] P. Villoresi, T. Jennewein, F. Tamburini, M. Aspelmeyer, C. Bonato, R. Ursin, C. Pernechele, V. Luceri, G. Bianco, A. Zeilinger, and C. Barbieri, Experimental verification of the feasibility of a quantum channel between space and earth, *New J. Phys.* **10**, 033038 (2008).
 - [7] J.-G. Ren, *et al.*, Ground-to-satellite quantum teleportation, *Nature* **549**, 70 (2017).
 - [8] Juan Yin, *et al.*, Entanglement-based secure quantum cryptography over 1,120 kilometres, *Nature* **582**, 501 (2020).
 - [9] Giuseppe Vallone, Davide Bacco, Daniele Dequal, Simone Gaiarin, Vincenza Luceri, Giuseppe Bianco, and Paolo

- Villoresi, Experimental Satellite Quantum Communications, *Phys. Rev. Lett.* **115**, 040502 (2015).
- [10] P. J. Shadbolt, M. R. Verde, A. Peruzzo, A. Politi, A. Laing, M. Lobino, J. C. F. Matthews, M. G. Thompson, and J. L. O'Brien, Generating, manipulating and measuring entanglement and mixture with a reconfigurable photonic circuit, *Nat. Photon* **6**, 4549 (2012).
- [11] Cristian Bonato, Markus Aspelmeyer, Thomas Jennewein, Claudio Pernechele, Paolo Villoresi, and Anton Zeilinger, Influence of satellite motion on polarization qubits in a space-earth quantum communication link, *Opt. Express* **14**, 10050 (2006).
- [12] Xuan Han, Hai-Lin Yong, Ping Xu, Kui-Xing Yang, Shuang-Lin Li, Wei-Yang Wang, Hua-Jian Xue, Feng-Zhi Li, Ji-Gang Ren, Cheng-Zhi Peng, and Jian-Wei Pan, Polarization design for ground-to-satellite quantum entanglement distribution, *Opt. Express* **28**, 369 (2020).
- [13] Vincenzo D'Ambrosio, Eleonora Nagali, Stephen P. Walborn, Leandro Aolita, Sergei Slussarenko, Lorenzo Marrucci, and Fabio Sciarrino, Complete experimental toolbox for alignment-free quantum communication, *Nat. Commun.* **3**, 961 (2012).
- [14] Ya-Ping Li, Wei Chen, Fang-Xiang Wang, Zhen-Qiang Yin, Li Zhang, Hang Liu, Shuang Wang, De-Yong He, Zheng Zhou, Guang-Can Guo, and Zheng-Fu Han, Experimental realization of a reference-frame-independent decoy bb84 quantum key distribution based on sagnac interferometer, *Opt. Lett.* **44**, 4523 (2019).
- [15] Ramy Tannous, Zhangdong Ye, Jeongwan Jin, Katanya B. Kuntz, Norbert Lütkenhaus, and Thomas Jennewein, Demonstration of a 6 state-4 state reference frame independent channel for quantum key distribution, *Appl. Phys. Lett.* **115**, 211103 (2019).
- [16] C. E. R. Souza, C. V. S. Borges, A. Z. Khoury, J. A. O. Huguenin, L. Aolita, and S. P. Walborn, Quantum key distribution without a shared reference frame, *Phys. Rev. A* **77**, 032345 (2008).
- [17] Anthony Laing, Valerio Scarani, John G. Rarity, and Jeremy L. O'Brien, Reference-frame-independent quantum key distribution, *Phys. Rev. A* **82**, 012304 (2010).
- [18] Teng-Yun Chen, Jun Zhang, J.-C. Boileau, Xian-Min Jin, Bin Yang, Qiang Zhang, Tao Yang, R. Laflamme, and Jian-Wei Pan, Experimental Quantum Communication Without a Shared Reference Frame, *Phys. Rev. Lett.* **96**, 150504 (2006).
- [19] F. Rezazadeh, A. Mani, and V. Karimipour, Quantum key distribution with no shared reference frame, *Quantum Inf. Proc.* **19**, 54 (2020).
- [20] Hongwei Liu, Jipeng Wang, and Haiqiang Ma Shihai Sun, Reference-Frame-Independent Quantum key Distribution Using Fewer States, *Phys. Rev. Appl.* **12**, 034039 (2019).
- [21] Peng-Liang Guo, Tao Li Qing Ai, and Fu-Guo Deng, Self-error-rejecting quantum state transmission of entangled photons for faithful quantum communication without calibrated reference frames, *EPL (Europhysics Letters)* **127**, 60001 (2019).
- [22] Juhwan Yoon, Tanumoy Pramanik, Byung-Kwon Park, Young-Wook Cho, Sang-Yun Lee, Sangin Kim, Sang-Wook Han, Sung Moon, and Yong-Su Kim, Experimental comparison of various quantum key distribution protocols under reference frame rotation and fluctuation, *Opt. Commun.* **441**, 64 (2019).
- [23] Yang Xue, Lei Shi, Jiahua Wei, Longqiang Yu, Huicun Yu, Jie Tang, and Zhaolei Zhang, Reference-frame-independent quantum key distribution in uplink and downlink free-space channel, *Int. J. Theor. Phys.* **59**, 3299 (2020).
- [24] Charles Bennett and Gilles Brassard, Quantum cryptography: Public key distribution and coin tossing, (IEEE, New York, 1984), p. 175.
- [25] Dagmar Bruß, Optimal Eavesdropping in Quantum Cryptography with six States, *Phys. Rev. Lett.* **81**, 3018 (1998).
- [26] Ryszard Horodecki, Paweł Horodecki, Michał Horodecki, and Karol Horodecki, Quantum entanglement, *Rev. Mod. Phys.* **81**, 865 (2009).
- [27] A. Barasiński, I. I. Arkhipov, and J. Svozilik, Localizable entanglement as a necessary resource of controlled quantum teleportation, *Sci. Rep.* **8**, 15209 (2018).
- [28] A. Barasiński, A. Černoč, and K. Lemr, Demonstration of Controlled Quantum Teleportation for Discrete Variables on Linear Optical Devices, *Phys. Rev. Lett.* **122**, 170501 (2019).
- [29] Zhao Wang, Chao Zhang, Yun-Feng Huang, Bi-Heng Liu, Chuan-Feng Li, and Guang-Can Guo, Experimental verification of genuine multipartite entanglement without shared reference frames, *Sci. Bulletin* **61**, 714 (2016).
- [30] Thomas Lawson, Anna Pappa, Boris Bourdoncle, Iordanis Kerenidis, Damian Markham, and Eleni Diamanti, Reliable experimental quantification of bipartite entanglement without reference frames, *Phys. Rev. A* **90**, 042336 (2014).
- [31] Shih-Xian Yang, Gelo Noel Tabia, Pei-Sheng Lin, and Yeong-Cherng Liang, Device-independent certification of multipartite entanglement using measurements performed in randomly chosen triads, *Phys. Rev. A* **102**, 022419 (2020).
- [32] Peter Shadbolt, Tamás Vértesi, Yeong-Cherng Liang, Cyril Branciard, Nicolas Brunner, and Jeremy L. O'Brien, Guaranteed violation of a bell inequality without aligned reference frames or calibrated devices, *Sci. Rep.* **2**, 470 (2012).
- [33] Joel J. Wallman and Stephen D. Bartlett, Observers can always generate nonlocal correlations without aligning measurements by covering all their bases, *Phys. Rev. A* **85**, 024101 (2012).
- [34] Y.-C. Liang, N. Harrigan, S. D. Bartlett, and T. Rudolph, Nonclassical Correlations from Randomly Chosen Local Measurements, *Phys. Rev. Lett.* **104**, 050401 (2010).
- [35] Artur Barasiński, Antonín Černoč, Karel Lemr, and Jan Soubusta, Genuine tripartite nonlocality for random measurements in greenberger-horne-zeilinger-class states and its experimental test, *Phys. Rev. A* **101**, 052109 (2020).
- [36] Minh Cong Tran, Borivoje Dakić, François Arnault, Wiesław Laskowski, and Tomasz Paterek, Quantum entanglement from random measurements, *Phys. Rev. A* **92**, 050301 (2015).
- [37] L. Knips, J. Dzierwior, W. Kłobus, T. Paterek W. Laskowski, P. J. Shadbolt, H. Weinfurter, and J. D. A. Meinecke, Multipartite entanglement analysis from random correlations, *npj Quantum Inf.* **6**, 51 (2020).
- [38] Wiesław Laskowski, Christian Schwemmer, Daniel Richart, Lukas Knips, Tomasz Paterek, and Harald Weinfurter, Optimized state-independent entanglement detection based on a

- geometrical threshold criterion, *Phys. Rev. A* **88**, 022327 (2013).
- [39] Karol Bartkiewicz, Grzegorz Chiriac, and Karel Lemr, Direct method for measuring and witnessing quantum entanglement of arbitrary two-qubit states through hong-ou-mandel interference, *Phys. Rev. A* **95**, 022331 (2017).
- [40] C. H. Bennett, D. P. DiVincenzo, J. A. Smolin, and W. K. Wootters, Mixed-state entanglement and quantum error correction, *Phys. Rev. A* **54**, 3824 (1996).
- [41] M. Horodecki and P. Horodecki, Reduction criterion of separability and limits for a class of distillation protocols, *Phys. Rev. A* **59**, 4206 (1999).
- [42] B. M. Terhal and K. G. H. Vollbrecht, Entanglement of Formation for Isotropic States, *Phys. Rev. Lett.* **85**, 2625 (2000).
- [43] F. Nosrati, A. Castellini, G. Compagno, and R. L. o Franco, Robust entanglement preparation against noise by controlling spatial indistinguishability, *npj Quantum Inf.* **6**, 39 (2020).
- [44] W. K. Wootters, Entanglement of Formation of an Arbitrary State of two Qubits, *Phys. Rev. Lett.* **80**, 2245 (1998).
- [45] Armin Uhlmann, Entropy and optimal decompositions of states relative to a maximal commutative subalgebra, *Open Syst. Inf. Dyn.* **5**, 209 (1998).
- [46] D. T. Pope and G. J. Milburn, Multipartite entanglement and quantum state exchange, *Phys. Rev. A* **67**, 052107 (2003).
- [47] P. Love, A. van den Brink, A. Smirnov, M. Amin, M. Grajcar, E. Ilichev, A. Izmailov, and A. Zagoskin, A characterization of global entanglement, *Quant. Inf. Proc.* **6**, 187 (2007).
- [48] Z.-H. Ma, Z.-H. Chen, J.-L. Chen, C. Spengler, A. Gabriel, and M. Huber, Measure of genuine multipartite entanglement with computable lower bounds, *Phys. Rev. A* **83**, 062325 (2011).
- [49] Zhi-Hua Chen, Zhi-Hao Ma, and Jing-Ling Chen, and Simone Severini, Improved lower bounds on genuine-multipartite-entanglement concurrence, *Phys. Rev. A* **85**, 062320 (2012).
- [50] T. Yu and J. H. Eberly, Evolution from entanglement to decoherence of bipartite mixed x states, *Quantum Inf. Comput.* **7**, 459 (2007).
- [51] S. M. Hashemi Rafsanjani, M. Huber, C. J. Broadbent, and J. H. Eberly, Genuinely multipartite concurrence of n-qubit x matrices, *Phys. Rev. A* **86**, 062303 (2012).
- [52] J. S. Bell, On the einstein podolsky rosen paradox, *Physics* **1**, 195 (1964).
- [53] J. F. Clauser, M. A. Horne, A. Shimony, and R. A. Holt, Proposed Experiment to Test Local Hidden-Variable Theories, *Phys. Rev. Lett.* **23**, 880 (1969).
- [54] I. Pitowsky and K. Svozil, Optimal tests of quantum nonlocality, *Phys. Rev. A* **64**, 014102 (2001).
- [55] C. Śliwa, Symmetries of the bell correlation inequalities, *Phys. Lett. A* **317**, 165 (2003).
- [56] J.-D. Bancal, J. Barrett, N. Gisin, and S. Pironio, Definitions of multipartite nonlocality, *Phys. Rev. A* **88**, 014102 (2013).
- [57] Valerio Scarani, The device-independent outlook on quantum physics, *Acta Phys. Slovaca* **62**, 347 (2012).
- [58] F. Verstraete and M. M. Wolf, Entanglement versus Bell Violations and Their Behavior under Local Filtering Operations, *Phys. Rev. Lett.* **89**, 170401 (2002).
- [59] S. Ghose, N. Sinclair, S. Debnath, P. Rungta, and R. Stock, Tripartite Entanglement versus Tripartite Nonlocality in Three-Qubit Greenberger-Horne-Zeilinger-Class States, *Phys. Rev. Lett.* **102**, 250404 (2009).
- [60] A. Barasiński, Restriction on the local realism violation in three-qubit states and its relation with tripartite entanglement, *Sci. Rep.* **8**, 12305 (2018).
- [61] H.-X. Lu, J.-Q. Zhao, X.-Q. Wang, and L.-Z. Cao, Experimental demonstration of tripartite entanglement versus tripartite nonlocality in three-qubit greenberger-horne-zeilinger-class states, *Phys. Rev. A* **84**, 012111 (2011).
- [62] J. J. Wallman, Y.-C. Liang, and S. D. Bartlett, Generating nonclassical correlations without fully aligning measurements, *Phys. Rev. A* **83**, 022110 (2011).
- [63] V. Lipinska, F. Curchod, A. Máttar, and A. Acín, Towards an equivalence between maximal entanglement and maximal quantum nonlocality, *New J. Phys.* **20**, 063043 (2018).
- [64] Artur Barasiński, Antonín Černoč, Wiesław Laskowski, Karel Lemr, Tamás Vértesi, and Jan Soubusta, Experimentally friendly approach towards nonlocal correlations in multisetting N-partite bell scenarios, *Quantum* **5**, 430 (2021).
- [65] Daniel F. V. James, Paul G. Kwiat, William J. Munro, and Andrew G. White, Measurement of qubits, *Phys. Rev. A* **64**, 052312 (2001).
- [66] Paul G. Kwiat, Klaus Mattle, Harald Weinfurter, Anton Zeilinger, Alexander V. Sergienko, and Yanhua Shih, New High-Intensity Source of Polarization-Entangled Photon Pairs, *Phys. Rev. Lett.* **75**, 4337 (1995).
- [67] Juan P. Torres, K. Banaszek, and I. A. Walmsley, Engineering nonlinear optic sources of photonic entanglement, *Progress in Optics* **56**, 227 (2011).
- [68] F. Bussi eres, C. Clausen, A. Tiranov, B. Korzh, V. B. Verma, S. W. Nam, F. Marsili, A. Ferrier, P. Goldner, H. Herrmann, C. Silberhorn, W. Sohler, M. Afzelius, and N. Gisin, Quantum teleportation from a telecom-wavelength photon to a solid-state quantum memory, *Nat. Photon* **8**, 775 (2014).
- [69] R. F. Werner, Quantum states with einstein-podolsky-rosen correlations admitting a hidden-variable model, *Phys. Rev. A* **40**, 4277 (1989).
- [70] Ll Masanes, Tight bell inequality for d-outcome measurements correlations, *Quantum Inf. Comput.* **3**, 345 (2003).
- [71] D. Collins and N. Gisin, A relevant two qubit bell inequality inequivalent to the CHSH inequality, *J. Phys. A* **37**, 1775 (2004).
- [72] C. Eltschka and J. Siewert, Entanglement of Three-Qubit Greenberger-Horne-Zeilinger-symmetric States, *Phys. Rev. Lett.* **108**, 020502 (2012).
- [73] K. Kraus, *States, Effects, and Operations: Fundamental Notions of Quantum Theory* (Springer-Verlag Berlin, Heidelberg, 1983).
- [74] J. Batle and M. Casas, Nonlocality and entanglement in qubit systems, *J. Phys. A: Math. Theor.* **44**, 445304 (2011).
- [75] K. H. Kagalwala, G. Di Giuseppe, A. F. Abouraddy, and B. E. Saleh, Bell's measure in classical optical coherence, (2013), - see example C.

- [76] W. J. Munro, D. F. V. James, A. G. White, and P. G. Kwiat, Maximizing the entanglement of two mixed qubits, *Phys. Rev. A* **64**, 030302 (2001).
- [77] Tzu-Chieh Wei, Kae Nemoto, Paul M. Goldbart, Paul G. Kwiat, William J. Munro, and Frank Verstraete, Maximal entanglement versus entropy for mixed quantum states, *Phys. Rev. A* **67**, 022110 (2003).
- [78] W. Dür and J. I. Cirac, Classification of multiqubit mixed states: Separability and distillability properties, *Phys. Rev. A* **61**, 042314 (2000).
- [79] A. Barasiński and J. Svozilík, Controlled teleportation of qubit states: Relation between teleportation faithfulness, controller's authority, and tripartite entanglement, *Phys. Rev. A* **99**, 012306 (2019).
- [80] O. Cohen and T. A. Brun, Distillation of Greenberger-Horne-Zeilinger States by Selective Information Manipulation, *Phys. Rev. Lett.* **84**, 5908 (2000).
- [81] W. Dür, G. Vidal, and J. I. Cirac, Three qubits can be entangled in two inequivalent ways, *Phys. Rev. A* **62**, 062314 (2000).
- [82] H. A. Carteret and A. Sudbery, Local symmetry properties of pure three-qubit states, *J. Phys. A* **33**, 4981 (2000).
- [83] Paul G. Kwiat, Edo Waks, Andrew G. White, Ian Appelbaum, and Philippe H. Eberhard, Ultrabright source of polarization-entangled photons, *Phys. Rev. A* **60**, R773 (1999).
- [84] See Supplemental Material at <http://link.aps.org/supplemental/10.1103/PhysRevApplied.16.054042> for experimental data.
- [85] E. Halenková, A. Černocho, K. Lemr, J. Soubusta, and S. Drusová, Experimental implementation of the multifunctional compact two-photon state analyzer, *Appl. Opt.* **51**, 474 (2012).
- [86] Z. Hradil, J. Řeháček, J. Fiurášek, and M. Ježek, in (*eds*) *Quantum State Estimation. Lecture Notes in Physics, vol 649*, edited by Paris M. and Řeháček J. (Springer, Berlin, Heidelberg, Oxford, 2004), Chap. chapter 3, p. 266..
- [87] A. Barasiński, A. Černocho, K. Lemr, and J. Soubusta, Experimental verification of time-order-dependent correlations in three-qubit greenberger-horne-zeilinger-class states, *Phys. Rev. A* **99**, 042123 (2019).
- [88] R. Horodecki, P. Horodecki, and M. Horodecki, Violating bell inequality by mixed spin-1/2 states: Necessary and sufficient condition, *Phys. Lett. A* **200**, 340 (1995).